130. Structural and Photophysical Properties of Lanthanide Nitrate 1:1 Complexes with Planar Tridentate Nitrogen Ligands Analogous to 2,2′:6′,2″-Terpyridine

by **Claude Piguet*** and **Alan F. Williams**

Department of Inorganic, Analytical and Applied Chemistry, University of Geneva, 30, quai Ernest Ansermet, CH–1211 Genève 4

and **Gérald Bernardinelli**

Laboratory of X-Ray Cystallography, University of Geneva, 30, quai Ernest Ansermet, CH–1211 Genève 4

and **Emmanuel Moret*** and **Jean-Claude G. Bünzli**

Institut of Analytical and Inorganic Chemistry, University of Lausanne, 3, place du Château, CH–1005 Lausanne

(29.IV.92)

The ligand 2,6-bis(1-methylbenzimidazol-2-yl)pyridine (mbzimpy, **1**) reacts with Eu^{III} to give $[Eu(mbzimpy)(NO_3)_3(CH_3OH)]$ [**4**] whose crystal structure ($EuC_{22}H_{21}N_8O_{10}$, $a = 7.658(3)$ Å, $b = 19.136(2)$ Å, $c = 8.882$ Å, $\beta = 104.07(1)°$, monoclinic, $P2_1$, $Z = 2$) shows a mononuclear structure where Eu^{III} is ten-coordinate by a meridional tridentate mbzimpy ligand, three bidentate nitrates, and one CH_3OH molecule, leading to a low-symmetry coordination sphere around the metal ion. Essentially the same coordination is found in the crystal structure of $[Eu(obzimpy)(NO_3)_3]$ (**8**) ($EuC_{35}H_{45}N_8O_9$, $a = 9.095(2)$ Å, $b = 16.624(2)$ Å, $c = 26.198(6)$ Å, $\beta = 95.85(1)°$, monoclinic, $P2_1/c$, $Z = 4$) obtained by reaction of 2,6-bis(1-octylbenzimidazol-2-yl)pyridine (obzimpy, **2**) with Eu^{III}. Detailed photophysical studies of crystalline $[Ln(mbzimpy)(NO_3)_3(CH_3OH)]$ and $[Ln(obzimpy)(NO_3)_3]$ complexes (Ln = Eu, Gd, Tb, Lu) show that **1** and **2** display $^1\pi\pi^*$ and $^3\pi\pi^*$ excited states very similar to those observed in 2,2′:6′,2″-terpyridine, leading to efficient ligand to Ln^{III} intramolecular energy transfer. Spectroscopic results show that an extremely efficient mbzimpy-to-Eu^{III} transfer occurs in $[Ln(mbzimpy)(NO_3)_3(CH_3OH)]$ and, in the case of Tb^{III}, a Tb^{III}-to-mbzimpy back transfer is also implied in the deactivation process. The origin of these peculiar effects and the influence of ligand design by going from mbzimpy to obzimpy are discussed. ^{1}H-NMR and luminescence data indicate that the structure found in the crystal is essentially maintained in solution.

Introduction. – The luminescent properties of lanthanide metal ions, in particular Eu^{III}, make them good candidates for use as spectroscopic probes and labels for a variety of chemical and biological applications [1]. In the last few years, there has been growing interest in the development of heterocyclic aromatic donor groups incorporated in macrocyclic [2], macrobicyclic [3], or podand-type [3] ligands capable of giving highly stable and strongly luminescent Eu^{III} and Tb^{III} complexes [4]. Although several complexes of lanthanides with 2,2′-bipyridine have been the subject of intensive research [2–5], less interest has been focused on 2,2′:6′,2″-terpyridine (terpy) derivatives which display similar photophysical properties [6] and also give coordination complexes with lanthanide metal ions [7]. Several workers have reported hydrated 1:1 complexes of 2,2′:6′,2″-terpyridine with almost all the lanthanides except radioactive Pm [8–10], but 1:2 stoichiometries are less common [8] [9], while $[Ln(terpy)_3]^{3+}$ with pseudo-D_3 symmetry may be

prepared in absence of coordinating counter-ions [11]. In CH_3CN solution, $[Eu(terpy)_3]^{3+}$ exhibits on-off equilibria of the pyridine rings giving a predominantly eight-coordinate complex [12]. The incorporation of terpyridyl moieties in multidentate ligands is synthetically more difficult than with 2,2′-bipyridine, and it is probably the reason for its rare use in supramolecular chemistry, although *Sauvage* and *Ward* have recently synthesized a catenand with two interlocked rings containing terpyridyl units [13]. However, we previously used the ligand 2,6-bis(1-methylbenzimidazol-2-yl)pyridine (mbzimpy, **1**), an analogue of 2,2′:6′,2″-terpyridine [14], as building block for self-assembly of helical Cu^I complexes [15], and we have incorporated this tridentate donor in multidentate ligands [16]. As an aspect of our interest in helical coordination complexes [15] [17], we have planned to use lanthanide ions as spectroscopic probes in dinuclear helical complexes with heterocyclic multidentate ligands as previously reported for macrocyclic *Schiff* bases [18]. As a first step towards this goal, we present here the synthesis and the photophysical properties of 1:1 complexes of the ligands **1** and 2,6-bis(1-octylbenzimidazol-2-yl)-pyridine (obzimpy, **2**) with lanthanide ions. A combined study of the Gd^{III}, Tb^{III}, and Eu^{III} complexes give information on the behaviour of the ligand-centered (LC), metal-centered (MC) levels, and the nature and efficiency of the energy-transfer processes between the ligand and the metal ion [4] [18]. The lowest excited state of Gd^{III} lies generally above the

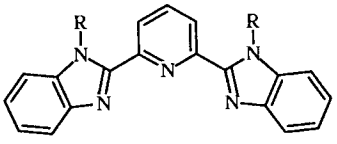

1 (mbzimpy) R = CH_3

2 (obzimpy) R = $CH_3(CH_2)_7$

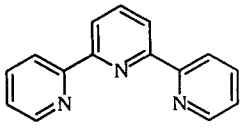

terpy

LC excited states and leads to the investigation of the fluorescence and phosphorescence of the coordinated ligand. Informations relevant to LC excited states may be obtained from Eu^{III} and Tb^{III} complexes where low luminescent MC levels can be populated through ligand excitation followed by energy transfer eventually leading to MC luminescence. A topic of considerable interest in this field is the use of direct energy transfer between Tb^{III} and Eu^{III} in mixed or doped complexes to evaluate the intermetallic distance [18] and to transfer photonic information. In this paper, we show that mononuclear complexes of **1** display a very unusual antenna effect [2–4] strongly dependent on the temperature. We report that a slight modification of the ligand allows a partial control of the energy migration in the crystal without significantly perturbing the coordination around the metal ion.

Experimental. – Solvents and starting materials were purchased from *Fluka AG* (Buchs, Switzerland) and used without further purification, unless otherwise stated. Aluminium oxide (*Merck* Act. II–III, 0.063–0.200 mm) was used for prep. column chromatography.

Preparation of the Ligands. The ligand 2,6-bis(1-methylbenzimidazol-2-yl)pyridine (mbzimpy, **1**) was prepared according to the method described in [14], but further purifications required for luminescence measurements were performed by column chromatography (Al_2O_3; CH_2Cl_2/MeOH 99:1) followed by crystallization from MeCN. The

ligand 2,6-bis(1-octylbenzimidazol-2-yl)pyridine (obzimpy, **2**) was obtained using the same procedure [14] with 1-octyl bromide as alkylating material (yield 82%). ^{1}H-NMR ($CDCl_3$): 0.75 (*t*, ^3J = 7, 6 H); 1.0 (*m*, 20 H); 1.55 (*quint.*, ^3J = 7, 4 H); 4.54 (*t*, ^3J = 7, 4 H); 7.4 (*m*, 6 H); 7.8 (*m*, 2 H); 8.05 (*t*, ^3J = 8, 1 H); 8.32 (*d*, ^3J = 8, 2 H).

Preparation of [Ln(mbzimpy)(NO$_3$)$_3$(CH$_3$OH)] (Ln = Nd, **3**; Ln = Eu, **4**; Ln = Gd, **5**; Ln = Tb, **6**; Ln = Lu, **7**) *and [Ln(obzimpy)(NO$_3$)$_3$]* (Ln = Eu, **8**; Ln = Gd, **9**; Ln = Lu, **10**). The nitrate salts $Ln(NO_3)_3 \cdot n H_2O$ (n = 5, 6) were prepared from the corresponding oxide (*Glucydur*, 99.99%) according to a literature method [19]. 0.339 g (1 mmol) of mbzimpy (**1**) in CH_2Cl_2 (7 ml) were slowly added to a soln. of $Ln(NO_3)_3$ (1 mmol) in MeCN (10 ml) under vigorous stirring. The CH_2Cl_2 was evaporated and the white precipitate was filtered, then suspended in hot MeCN for 2 h. After cooling, the crude precipitate was separated, dried under vacuum, and recrystallized from hot CH_3OH to give crystals of [Ln(mbzimpy)$(NO_3)_3(CH_3OH)$] (Ln = Nd, **3**; Ln = Eu, **4**; Ln = Gd, **5**; Ln = Tb, **6**; Ln = Lu, **7**) in 80–90% yield. X-Ray-quality crystals were obtained by slow diffusion of Et_2O into a concentrated soln. of **4** in MeOH. The same procedure was used with **2** except that the crude complexes were recrystallized from MeCN to give X-ray-quality pale yellows prisms of [Ln(obzimpy)$(NO_3)_3$] (Ln = Eu, **8**; Ln = Gd, **9**; Ln = Lu, **10**) in 60–80% yield. All these complexes were characterized by their IR spectra and gave satisfactory elemental analyses. Eu-doped (0.1–2%) or Tb-doped (2%) compounds were prepared according to the same procedure using stoichiometric mixtures of lanthanide nitrate salts.

Crystal-Structure Determination of [Eu(mbzimpy)(NO$_3$)$_3$(CH$_3$OH)] (**4**) *and [Eu(obzimpy)(NO$_3$)$_3$]* (**8**). Crystal data and details of intensity measurements and structure refinements are given in *Table 1*. Cell dimensions

Table 1. *Crystal Data, Intensity Measurements, and Structure Refinement for [Eu(mbzimpy)(NO$_3$)$_3$(CH$_3$OH)]* (**4**) *and [Eu(obzimpy)(NO$_3$)$_3$]* (**8**)

Compound	**4**	**8**
Formula	$Eu(C_{21}H_{17}N_5)(NO_3)_3(CH_3OH)$	$Eu(C_{35}H_{45}N_5)(NO_3)_3$
Mol. wt.	709.4	873.7
Crystal size	0.05 × 0.14 × 0.14 mm	0.20 × 0.20 × 0.25
Crystal system	monoclinic	monoclinic
Space group	$P2_1$	$P2_1/c$
a [Å]	7.658(3)	9.095(2)
b [Å]	19.136(2)	16.624(2)
c [Å]	8.882(2)	26.198(6)
β [deg]	104.07(1)	95.85(1)
V [Å^3]	1262.6(6)	3940(1)
F_{000}	704	1784
Z	2	4
D_{calc} [g·cm^{-3}]	1.87	1.47
Radiation	MoK_α (0.71069 Å)	MoK_α (0.71069 Å)
μ [mm^{-1}]	2.557	1.651
Min. and max. A* [20]	1.127, 1.398	1.275, 1.380
hkl range	–8 to 8, 0 to 21, 0 to 10 and all anti-reflections	–9 to 9, 0 to 17, 0 to 26
$\sin(\theta/\lambda)_{max}$ [Å^{-1}]	0.58	0.53
R_{int}	0.028	0.026
No. of measured reflections	4350	4939
No. of observed reflections	4027	3568
Criterion for observed reflections	$\|F_o\| > 4\sigma(F_o)$	$\|F_o\| > 4\sigma(F_o)$
Refinement (on F)	full-matrix	full-matrix
No. of parameters	370	470
Weight function	$1/\sigma^2(F_o)$	1
Enantiomorph polarity (x) [25]	–0.01(2)	–
Max. and min. $\Delta\rho$, [e Å^{-3}]	0.63, –0.85	1.25, –1.09
Max. and average Δ/σ	0.16 10–3, 0.93 10–3	1.13, 0.033 (disordered sites)
S	1.19	3.43
R, R_w	0.038, 0.033	0.046, 0.046

and intensities were measured at r.t. on *Nonius CAD4* (for **4**) and *Philips PW1100* (for **8**) diffractometers. Data were corrected for *Lorentz* polarization and for absorption effects [20]. The structures were solved by direct methods using MULTAN 87 [21]; all other calculations used XTAL [22] system and ORTEP II [23] programs. Atomic scattering factors and anomalous dispersion terms were taken from [24]. All coordinates of H-atoms were calculated. For **4**, the absolute configuration has been established by refinement of the enantiomorph-polarity parameter [25] ($x = -0.01(2)$). The structure of the complex **8** shows a slight disorder on the three terminal C-atoms of one of the octyl chains. This disorder has been resolved, and six atomic sites have been observed (*cf. Fig. 5*) and refined with isotropic atomic displacement parameters and site occupancy factors of 0.5. All other non-H-atoms were refined with anisotropic atomic displacement parameters. The final *Fourier* difference synthesis showed, for both structures, a residual electronic density (*ca.* ± 1 eÅ^{-3}) in the vicinity of the Eu-atom.

Physical Measurements. Electronic spectra in the UV/VIS range were recorded in soln. with a *Perkin-Elmer Lambda 5* spectrophotometer at 20° using quartz cells of 0.1-cm path length and in solid state with a *Perkin-Elmer Hitachi 340* spectrophotometer using MgO dispersions. IR spectra were obtained from KBr or polyethylene pellets with *Perkin-Elmer IR 597* and *FT-Bruker IFS-113V* spectrophotometers. ^{1}H-NMR spectra were recorded on a *Bruker AMX 400* spectrometer. Chemical shifts δ are given in ppm *vs.* TMS. The experimental procedures for high-resolution, laser-excited luminescence experiments have been published in [26]. Elemental analyses were performed by Dr. *H. Eder* of the Microchemical Laboratory of the University of Geneva. Metal contents were determined by ICP (*Perkin-Elmer Plasma 1000*) after acidic oxidative mineralization of the complex.

Results and Discussions. – *Preparation of Compounds.* The lanthanide complexes are prepared by mixing the ligands **1** or **2** with stoichiometric amounts of $Ln(NO_3)_3 \cdot nH_2O$ [19] in CH_2Cl_2/CH_3CN (Ln = Nd, Eu, Gd, Tb, Lu). With **1**, a crude precipitate containing H_2O may be easily recrystallized from hot CH_3OH to give the nitrate complexes whose elemental analyses are fully compatible with the formulation $[Ln(mbzimpy)(NO_3)_3(CH_3OH)]$ (Ln = Nd, **3**; Ln = Eu, **4**; Ln = Gd, **5**; Ln = Tb, **6**; Ln = Lu, **7**). The use of the lipophilic ligand **2** results in the formation of complexes which are more soluble in organic solvents and may be crystallized from MeCN solutions to give pale yellow prisms whose elemental analyses correspond to $[Ln(obzimpy)(NO_3)_3]$ (Ln = Eu, **8**; Lu = Gd, **9**; Ln = Lu, **10**). The IR spectra of complexes **3–10** are very similar to those reported [8] for $[Ln(terpy)(NO_3)_3]$ (Ln = Tb–Yb) and show characteristic ligand vibrations in the range 1600–1500 cm^{-1} (C=C, C=N stretching) which are slightly shifted toward high energy (5–10 cm^{-1}) upon complexation as previously observed for Cu^{I} [15], Cu^{II}, and Zn^{II} [14] complexes of mbzimpy (**1**). The nitrates show four absorptions in the range 1600–800 cm^{-1} which are typical for coordinated NO_3 groups [27] and may be easily attributed to out-of-plane rocking (810–812 cm^{-1}; ν_6) and to the three stretching modes 1028–1035 cm^{-1} (ν_2), 1288–1295 cm^{-1} (ν_4), and 1470–1490 cm^{-1} (ν_1). The two vibration modes expected [8] [18] [27] in the range 750–700 cm^{-1} (ν_3, ν_5) are masked by out-of-plane bending of the aromatic ligands appearing in this region [28]. The separation of the two highest frequency bands (ν_1) lies in the range 175–190 cm^{-1} for complexes **3–10** strongly suggesting symmetrically bidentate NO_3 groups [27] [29]. This conclusion is supported by the large splitting found for the combination band $\nu_1 + \nu_4$ (35–45 cm^{-1}) [30] in the IR spectra. The stretching vibrations Eu–N(ligand) appear near 200 cm^{-1} for complex **4** while Eu–O stretching vibrations give a broad band in the range 200–150 cm^{-1} in good agreement with the 160 cm^{-1} broad band found in $[Eu(H_2O)_4(NO_3)_3]$. These results strongly suggest that the ligands **1** and **2** are meridionally tricoordinated to Ln^{III} in a similar fashion as previously observed with Cu^{II} [14] [31], and that each NO_3 group adopts a bidentate coordination mode.

X-Ray Crystal Structure of [Eu(mbzimpy)(NO$_3$)$_3$(CH$_3$OH)] (**4**). Selected bond distances, angles, and least-squares-plane data for complex **4** are given in *Table 2. Fig. 1*

Table 2. *Selected Bond Distances* [Å] *and Angles* [°], *and Least-Squares-Plane Data for* $[Eu(mbzimpy)(NO_3)_3(CH_3OH)]$ (**4**)

Distances [Å]

Eu–N(1)	2.477(7)	Eu–O(301)	2.474(8)	N(201)–O(202)	1.27(1)
Eu–N(3)	2.611(7)	Eu–O(302)	2.498(8)	N(201)–O(203)	1.24(1)
Eu–N(4)	2.537(9)	Eu–O(001)	2.494(7)	N(301)–O(301)	1.29(1)
Eu–O(101)	2.453(7)	N(101)–O(101)	1.27(1)	N(301)–O(302)	1.24(1)
Eu–O(102)	2.535(7)	N(101)–O(102)	1.23(1)	N(301)–O(303)	1.19(1)
Eu–O(201)	2.68(1)	N(101)–O(103)	1.25(1)	O(001)–C(01)	1.44(1)
Eu–O(202)	2.478(7)	N(201)–O(201)	1.26(1)		

Angles [°]

N(1)–Eu–N(3)	62.7(3)	O(101)–Eu–O(301)	75.6(3)
N(1)–Eu–N(4)	125.5(2)	O(101)–Eu–O(302)	124.0(2)
N(1)–Eu–O(101)	139.2(2)	O(101)–Eu–O(001)	114.4(2)
N(1)–Eu–O(102)	111.4(3)	O(102)–Eu–O(201)	67.1(3)
N(1)–Eu–O(201)	69.9(3)	O(102)–Eu–O(202)	108.4(2)
N(1)–Eu–O(202)	77.4(2)	O(102)–Eu–O(301)	70.6(3)
N(1)–Eu–O(301)	138.9(3)	O(102)–Eu–O(302)	112.7(2)
N(1)–Eu–O(302)	96.4(3)	O(102)–Eu–O(001)	64.7(2)
N(1)–Eu–O(001)	71.7(2)	O(201)–Eu–O(202)	49.4(3)
N(3)–Eu–N(4)	63.6(2)	O(201)–Eu–O(301)	136.2(3)
N(3)–Eu–O(101)	132.3(2)	O(201)–Eu–O(302)	163.9(3)
N(3)–Eu–O(102)	173.8(2)	O(201)–Eu–O(001)	98.1(3)
N(3)–Eu–O(201)	108.1(2)	O(202)–Eu–O(301)	142.8(3)
N(3)–Eu–O(202)	69.4(2)	O(202)–Eu–O(302)	137.7(2)
N(3)–Eu–O(301)	114.8(3)	O(202)–Eu–O(001)	141.8(2)
N(3)–Eu–O(302)	70.7(2)	O(301)–Eu–O(302)	50.8(3)
N(3)–Eu–O(001)	113.1(2)	O(301)–Eu–O(001)	73.1(3)
N(4)–Eu–O(101)	77.1(2)	O(302)–Eu–O(001)	68.8(2)
N(4)–Eu–O(102)	122.0(3)	O(101)–N(101)–O(102)	117.6(8)
N(4)–Eu–O(201)	120.8(3)	O(101)–N(101)–O(103)	120(1)
N(4)–Eu–O(202)	76.5(2)	O(102)–N(101)–O(103)	122.9(9)
N(4)–Eu–O(301)	73.8(3)	O(201)–N(201)–O(202)	117.4(9)
N(4)–Eu–O(302)	73.7(3)	O(201)–N(201)–O(203)	122(1)
N(4)–Eu–O(001)	140.5(2)	O(202)–N(201)–O(203)	120.9(9)
O(101)–Eu–O(102)	50.8(3)	O(301)–N(301)–O(302)	115.0(9)
O(101)–Eu–O(201)	69.3(3)	O(301)–N(301)–O(303)	119.8(9)
O(101)–Eu–O(202)	76.3(2)	O(302)–N(301)–O(303)	125(1)

Least-squares planes

Description	*Deviations* [Å] Max.	Atom
1 Eu, N(1), N(3), N(4), O(102)	0.180	N(4)
2 benzimidazole, N(1), N(2)	0.027	C(1)
3 pyridine, N(3)	0.035	C(11)
4 benzimidazole, N(4), N(5)	0.022	C(15)
5 nitrate, N(101)	0.003	N(101)
6 nitrate, N(201)	0.002	N(201)
7 nitrate, N(301)	0.006	N(301)

Interplane angles [°]	2	3	4	5	6	7
1	7.4(2)	1.6(3)	7.7(2)	33.5(3)	76.7(3)	102.8(4)
2		6.5(3)	4.5(2)	40.5(3)	74.2(4)	110.2(4)
3			6.2(3)	34.0(4)	77.5(4)	103.8(4)
4				38.3(3)	78.7(3)	108.9(4)
5					99.7(4)	71.1(4)
6						114.7(4)

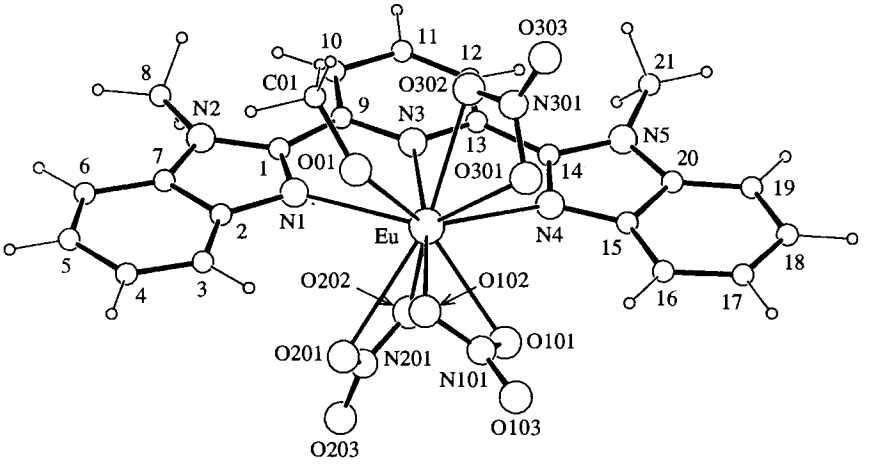

Fig. 1. *Atomic-numbering scheme for [Eu(mbzimpy)(NO$_3$)$_3$(CH$_3$OH)]* (**4**)

shows the atomic numbering scheme. *Fig. 2* gives ORTEP [23] stereoscopic view of the complex, and *Fig. 3* gives a view along the Eu–O(102) direction.

In agreement with the IR results, the crystal structure of **4** shows it to be composed of neutral complexes [Eu(mbzimpy)(NO$_3$)$_3$(CH$_3$OH)] where Eu^{III} is ten-coordinate by three

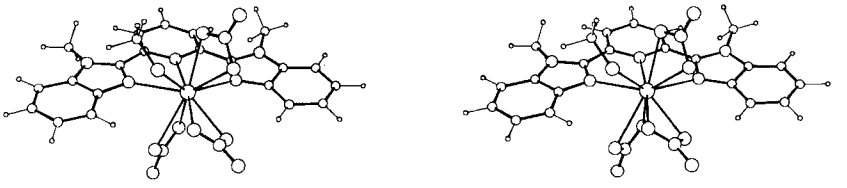

Fig. 2. *ORTEP* [23] *stereoscopic view of complex* **4**

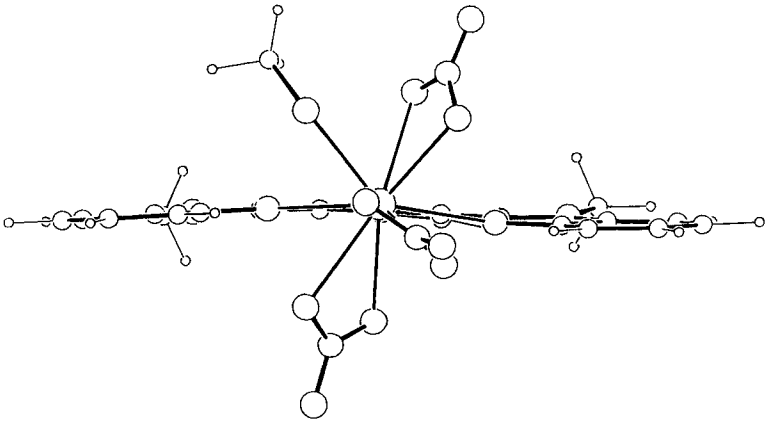

Fig. 3. *View of the complex* **4** *approximately in the plane of the mbzimpy ligand*

heterocyclic N-atoms of the mbzimpy ligand, six O-atoms of three bidentate NO_3 groups, and one molecule of CH_3OH. The mbzimpy (**1**) ligand is almost planar showing only small dihedral angles between the aromatic benzimidazole and pyridine rings (6.5(3)°, 6.2(3)°), and it adopts a *cis-cis*-conformation [32] [33] leading to a planar meridional coordination of the Eu-atom which lies approximately in a basal plane defined by the tricoordinated N-atoms of **1** and one O-atom (O(102)) belonging to a bidentate nitrate. Ligand **1** is asymmetrically bound to Eu^{III} in complex **4**, displaying two short Eu–N(benzimidazole) distances (2.537(9) Å, 2.477(7) Å) and one longer Eu–N(pyridine) distance (2.611(7) Å). These observations strongly contrast with the usual coordination of **1** [31] [34] or terpy [7] to transition-metal ions where the central pyridine is more tightly bound than the two aromatic side arms; but the larger ionic radius [35] of Eu^{III} probably prevents it entering into the ligand cavity which results in a long Eu–N(central pyridine) distance as previously found in [Eu(terpy)(DPM)$_3$] [10] (DPM = dipivaloylmethane). However, the mean Eu–N distance (2.54(6) Å) found in complex **4** is significantly shorter than those reported for [Eu(terpy)(DPM)$_3$] (2.65(1) Å) [10] and [Eu(terpy)$_3$(ClO$_4$)$_3$] (2.60 Å) [11] which suggests that the replacement of the pyridine side arms in terpy (six-membered ring) by imidazole derivatives in mbzimpy (**1**) (five-membered ring) slightly increases the size of the cavity allowing a closer approach of the Eu^{III}. Consequently, the two bite angles N(1)–Eu–N(2) (63.6(2)°) and N(1)–Eu–N(3) (62.7(3)°) are greater in complex **4** than in [Eu(terpy)(DPM)$_3$] [10]. All three NO_3 groups display approximate C_{2v} local symmetry with distortions due to the complexation [36]. One NO_3 is situated near the basal plane with one O-atom (O(102)) in the plane and the second O-atom (O(101)) coordinated to Eu^{III} just below this plane leading to a dihedral angle of 33.5(3)° between the NO_3 and the $EuN_3O(102)$ planes (*Fig. 3*). The two other NO_3 groups are located on each side of the $EuN_3O(102)$ basal plane, and the CH_3OH molecule occupies the tenth coordination site near a NO_3 group in a very similar way as recently described for [Eu(L)(NO$_3$)$_2$(CH$_3$OH)](NO$_3$) where L is a pentadentate *Schiff* base [37]. The Eu–O distances in complex **4** do not significantly deviate from the average value (2.52(8) Å) except Eu–O(201) (2.68(1) Å) which is 0.20(1) Å longer than the other Eu–O(202) distance giving an asymmetrically bound bidentate NO_3 which likely results from

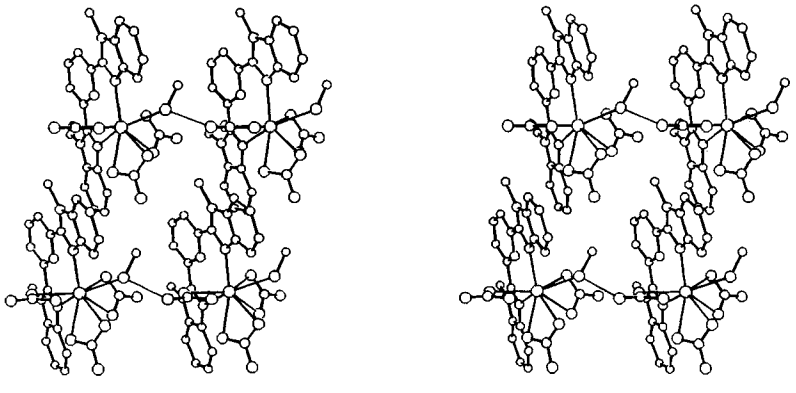

Fig. 4. *ORTEP* [23] *stereoscopic view along the* b *axis of four [Eu(mbzimpy)(NO$_3$)$_3$(CH$_3$OH)] units showing intermolecular stacking interactions and H-bonding* (along *a* axis) *in* **4**

H-bonding [38] between the free O-atom (O(203)) of this NO_3 group and the coordinated CH_3OH molecule of another molecule in the cell (O(203)···O(01) $x-1, y, z$ = 2.90(1) Å, *Fig. 4*).

In complex **4**, the mbzimpy ligands are packed in layers running roughly perpendicular to the *b* axis and producing slipped stacks of approximately parallel ligand molecules in a similar fashion to that found in crystals of aromatic molecules such as 2,2′-bipyridine [39] or 2,2′:6′,2″:6″,2‴-quaterpyridine [40]. These layers are stacked along the *b* axis in an alternative mode giving a zig-zag arrangement of the planar aromatic mbzimpy ligands. *Fig. 4* illustrates the two type of interactions observed between neighboring molecules within a layer. Stacking interactions are found between the pyridine ring of one molecule of **4** and a benzimidazole ring belonging to a different unit translated along *c*. The two aromatic planes are almost parallel (6.1(4)°) with a contact distance (3.53–3.70 Å) compatible with aromatic stacking interactions.

X-Ray Crystal Structure of [Eu(obzimpy)(NO$_3$)$_3$] (**8**). Selected bond distances, angles, and least-squares plane data for complex **8** are given in *Table 3*. *Fig. 5* shows the atomic numbering scheme. *Fig. 6* gives ORTEP [23] stereoscopic view of the complex in the same orientation as complex **4** in *Fig. 2*.

Table 3. *Selected Bond Distances* [Å] *and Angles* [°], *and Least-Squares Plane Data for [Eu(obzimpy)(NO$_3$)$_3$]* (**8**)

Distances [Å]					
Eu–N(1)	2.491(7)	Eu–O(202)	2.497(8)	N(201)–O(201)	1.23(1)
Eu–N(3)	2.598(7)	Eu–O(301)	2.434(8)	N(201)–O(202)	1.25(1)
Eu–N(4)	2.473(8)	Eu–O(302)	2.476(9)	N(201)–O(203)	1.23(2)
Eu–O(101)	2.463(7)	N(101)–O(101)	1.24(1)	N(301)–O(301)	1.26(1)
Eu–O(102)	2.447(7)	N(101)–O(102)	1.27(1)	N(301)–O(302)	1.25(1)
Eu–O(201)	2.450(9)	N(101)–O(103)	1.20(1)	N(301)–O(303)	1.23(2)

Angles [°]			
N(1)–Eu–N(3)	64.1(2)	O(101)–Eu–O(202)	71.2(3)
N(1)–Eu–N(4)	128.3(2)	O(101)–Eu–O(301)	113.8(3)
N(1)–Eu–O(101)	128.3(2)	O(101)–Eu–O(302)	68.3(3)
N(1)–Eu–O(102)	83.9(2)	O(102)–Eu–O(201)	114.0(3)
N(1)–Eu–O(201)	109.2(3)	O(102)–Eu–O(202)	75.4(3)
N(1)–Eu–O(202)	73.5(3)	O(102)–Eu–O(301)	84.5(3)
N(1)–Eu–O(301)	81.0(3)	O(102)–Eu–O(302)	73.3(3)
N(1)–Eu–O(302)	128.0(3)	O(201)–Eu–O(202)	50.8(3)
N(3)–Eu–N(4)	64.4(2)	O(201)–Eu–O(301)	159.2(3)
N(3)–Eu–N(101)	164.5(2)	O(201)–Eu–O(302)	122.7(3)
N(3)–Eu–O(102)	144.0(2)	O(202)–Eu–O(301)	148.9(3)
N(3)–Eu–O(201)	92.7(3)	O(202)–Eu–O(302)	138.7(3)
N(3)–Eu–O(202)	108.0(3)	O(301)–Eu–O(302)	51.4(3)
N(3)–Eu–O(301)	75.2(3)	O(101)–N(101)–O(102)	116.2(7)
N(3)–Eu–O(302)	113.2(3)	O(101)–N(101)–O(103)	122.6(9)
N(4)–Eu–O(101)	102.1(3)	O(102)–N(101)–O(103)	121.2(9)
N(4)–Eu–O(102)	145.8(3)	O(201)–N(201)–O(202)	117(1)
N(4)–Eu–O(201)	70.0(3)	O(201)–N(201)–O(203)	121(1)
N(4)–Eu–O(202)	120.4(3)	O(202)–N(201)–O(203)	122(1)
N(4)–Eu–O(301)	89.4(3)	O(301)–N(301)–O(302)	116(1)
N(4)–Eu–O(302)	76.7(3)	O(301)–N(301)–O(303)	122(1)
O(101)–Eu–O(102)	51.4(2)	O(302)–N(301)–O(303)	122(1)
O(101)–Eu–O(201)	74.7(3)		

Table 3 (cont.)

Least-squares planes Description				*Deviations* [Å] Max.		Atom
1 Eu, N(1), N(3), N(4), O(101)				0.226		O(101)
2 benzimidazole, N(1), N(2)				0.024		N(1)
3 pyridine, N(3)				0.026		C(8)
4 benzimidazole, N(4), N(5)				0.033		C(17)
5 nitrate, N(101)				0.002		N(101)
6 nitrate, N(201)				0.015		N(201)
7 nitrate, N(301)				0.003		N(301)
Interplane angles [°]	2	3	4	5	6	7
1	17.1(2)	19.5(3)	18.3(2)	28.4(3)	109.7(4)	92.2(4)
2		29.0(3)	34.6(2)	45.2(3)	100.2(4)	102.4(4)
3			28.3(2)	33.0(4)	128.3(4)	103.5(5)
4				10.9(9)	111.1(4)	76.1(5)
5					116.3(5)	70.6(5)
6						69.8(5)

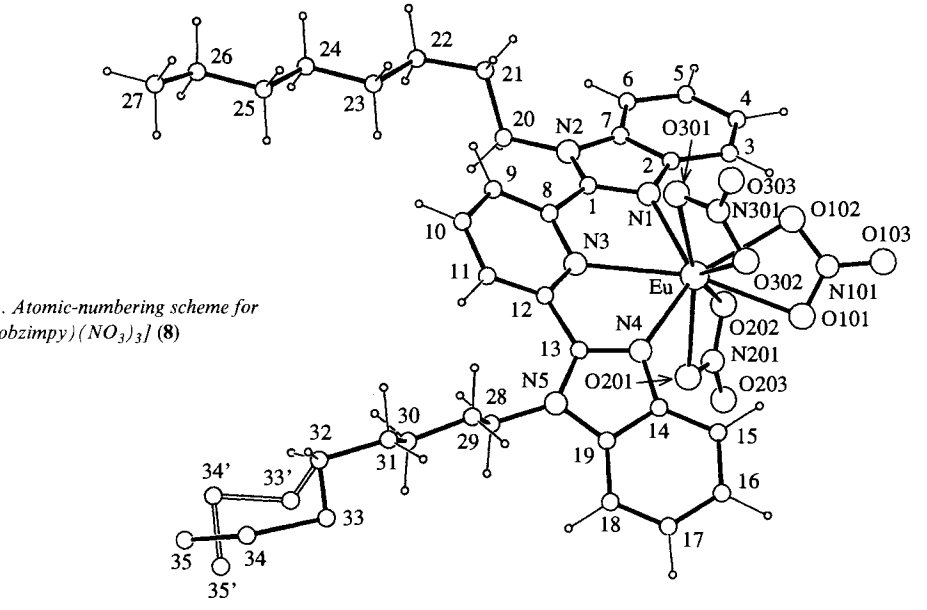

Fig. 5. *Atomic-numbering scheme for [Eu(obzimpy)(NO$_3$)$_3$]* (**8**)

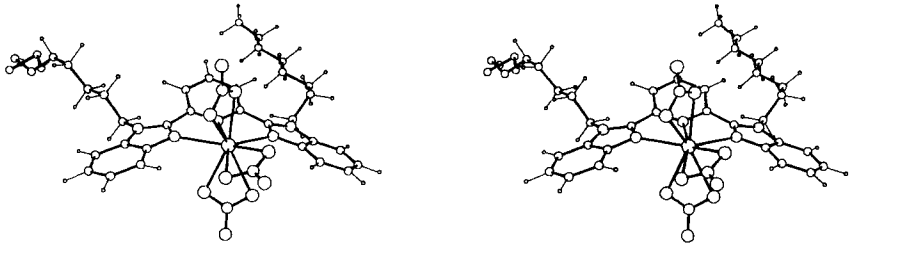

Fig. 6. *ORTEP* [23] *stereoscopic view of complex* **8**

The structure of **8** shows a neutral complex [Eu(obzimpy$(NO_3)_3$] whose geometrical characteristics are similar to those observed for complex **4**, but Eu^{III} is only nine-coordinated in **8**, because no solvent molecule is bound to the metal ion. As in complex **4**, the Eu-atom lies in a basal plane defined by the tricoordinated N-atoms of obzimpy (**2**) and one O-atom O(102) belonging to a bidentate NO_3; the two remaining bidentate NO_3 groups being located on either side of this plane. The mean Eu–N distance (2.52(7) Å) is comparable to that found in complex **4**, but the tridentate ligand is no longer planar and adopts a bent conformation showing significant dihedral angles (29.7(3)°, 28.3(3)°) between the central pyridine ring and the aromatic benzimidazole side arms. As observed for **4**, the obzimpy ligand in **8** is bound to Eu^{III} with one long Eu–N(pyridine) distance (2.598(7) Å) and two shorter Eu–N(benzimidazole) distances (2.491(7) Å, 2.473(8) Å). The Eu–O distances show only small deviations from the mean value (2.46(2) Å) indicating the presence of three roughly symmetrically bound bidentate NO_3 groups in **8**. If we neglect the coordinated CH_3OH molecule in **4**, the geometries around the Eu-atom are similar for both complexes, the principal difference arising from the bent conformation of the ligand obzimpy in **8**. As expected from ligand design, upon coordination to europium the lipophilic octyl chains in obzimpy (**2**) are directed away from the metal ion and do not interfere with the coordination sphere around Eu^{III}, but strongly affect the crystal packing. The bent obzimpy ligands are packed in layers along the *c* axis, each layer running approximately along the *b* axis (*Fig. 7*).

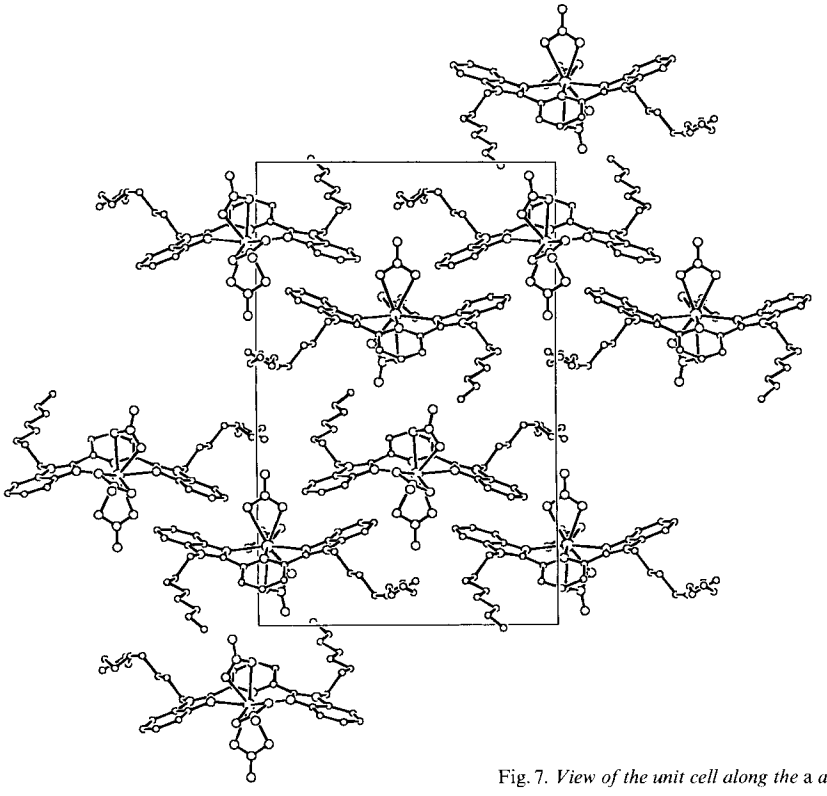

Fig. 7. *View of the unit cell along the* a *axis in* **8**

Within one layer, the [Eu(obzimpy)$(NO_3)_3$] molecules adopt a disposition where one convex-bent obzimpy ligand alternates with a concave-bent obzimpy ligand eventually leading to an undulating arrangement running in the *b* direction. The benzimidazole rings of two alternated concave and convex units are almost parallel (7.2°, 6.6°) showing a head-to-tail arrangement of the benzimidazole moieties. Contact distances between the benzimidazole rings lie in the range of 3.35–3.90 Å which are compatible with aromatic stacking interactions despite a very poor overlap between the aromatic rings.

In conclusion, both complexes **4** and **8** show similar low-symmetry coordination geometries around Eu^{III} with a meridionally coordinated tridentate aromatic ligand and three bidentate NO_3 groups, but the introduction of lipophilic octyl chains in **8** strongly modifies the crystal packing and, consequently, the weak observed intermolecular interactions. The H-bonds between [Eu(mbzimpy)$(NO_3)_3(CH_3OH)$] in crystals of **4** disappear in complex **8**, and the aromatic intermolecular stacking interactions between the central pyridine ring and the benzimidazole ring of two different mbzimpy ligands in **4** are no longer observed in complex **8** where the bent obzimpy ligands show only weak intermolecular aromatic stacking interactions between the benzimidazole moieties. The effective ionic radius of the Eu^{III} ion can be calculated using *Shannon*'s definition [35] and $r(O) = 1.31$ Å and $r(N) = 1.46$ Å [26]. It amounts to 1.17 Å and 1.12 Å in **4** and **8**, respectively. These values are in perfect agreement with those reported for ten- and nine-coordinate Eu^{III} complexes (1.18 and 1.12 Å [5], respectively).

Photophysical Properties of Ligands mbzimpy (**1**) *and obzimpy* (**2**) *and Their Complexes with* Ln^{III} (**3–10**) *in the Solid State. Electronic Properties of* **1** *and* **2**. According to *Nakamoto* [32], the strong absorption displayed in the reflectance spectrum of free mbzimpy (**1**) around 27800 cm^{-1} may be attributed to a $\pi_1 \rightarrow \pi^*$ transition. Upon complexation to Eu^{III}, the latter splits into two components, $\pi_1^a \rightarrow \pi^*$ at *ca.* 28750 cm^{-1} and $\pi_1^b \rightarrow \pi^*$ at *ca.* 26320 cm^{-1} in [Eu(mbzimpy)$(NO_3)_3(CH_3OH)$] (**4**) and [Eu(obzimpy$(NO_3)_3$] (**8**), as previously described, when such ligands are meridionally coordinated to metal ions [14] [15] [32]. The reflectance spectra of Ln-mbzimpy do not show any particular individual effect such as charge-transfer absorption upon Ln variation (Ln = Eu, Gd, Tb, Lu), f→f transitions of very low intensity are, however, observed in the Eu^{III} or Tb^{III} complexes.

The emission spectra measured at 295 K for mbzimpy (**1**) and Ln-mbzimpy complexes **5** (Ln = Gd) and **7** (Ln = Lu) upon ligand-excitation (340 nm) show intense asymmetric broad bands which are assigned to ligand luminescence (400–450 nm; *Fig. 8*). Their maxima are situated at 26040 and 23530 cm^{-1}, respectively, and a shoulder is observed on the red side of the free ligand spectrum (21050 cm^{-1}). The excitation spectra measured upon monitoring these emission bands (*Fig. 8*, dashed line) are similar to those reported for bpy and La-tris-bpy cryptate [41]: they confirm the splitting of the ligand electronic levels induced by the coordination (*cf.* reflectance spectra). The maxima of these excitation bands do not correspond to those observed in absorption measurements, because saturation phenomena and the instrumental response alter the shape of the spectra below 400 nm. The relatively small *Stokes* shift (*ca.* 1500–2200 cm^{-1}, estimated from absorption and emission maxima) lead us to assign the observed emission bands to $^1\pi\pi^*$ transitions. This conclusion is confirmed by the very fast decay of the emitted light (non-exponential decays in the range of ns were observed).

Under similar experimental conditions, very different emission spectra are observed with Eu- and Tb-mbzimpy complexes **4** and **6**, respectively: the ligand-fluorescence band

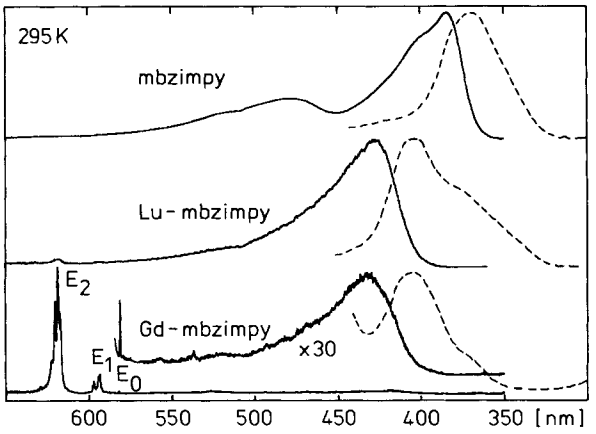

Fig. 8. *Luminescence spectra of mbzimpy, [Lu(mbzimpy)(NO$_3$)$_3$(CH$_3$OH)]* (**7**) *and [Gd(mbzimpy)(NO$_3$)$_3$(CH$_3$OH)]* **5** *at 295 K. Full lines*: emission spectra (λ_{exc} = 340 nm); $E_J = {}^5D_0 \rightarrow {}^7F_J$ (Eu) transitions. *Dashed lines*: excitation spectra (λ_{an} = 385 nm (free ligand) and 425 nm (complexes)).

vanishes completely, and the spectra only comprise strong narrow lines originating from f→f transitions (*cf. Figs. 10* and *11*). As observed in Ln-bpy cryptates [41–43] or Ln-terpy complexes [9] [11], this points to an efficient conversion of the UV light absorbed by the mbzimpy ligand into visible luminescence of the lanthanide ions.

A remarkable effect is observed in Gd- and Tb-mbzimpy complexes **5** and **6**, respectively, which explains the unexpected red and orange colors, respectively, emitted by these samples when placed under UV irradiation: in spite of the high purity of the starting oxides (99.99%), strong emission lines originating from traces of Eu^{III} are measured. No precise elemental analysis was made to check the percentage of Eu^{III} included in these samples, but any accidental contamination could be exluded on the following grounds: *1*) The same results were obtained with independently synthesized complexes using different 99.99% pure samples of Gd and Tb oxides. *2*) No Eu^{III} emission was observed with the Gd-obzimpy complex **9** prepared with the same starting lanthanide nitrate as Gd-mbzimpy **5**. *3*) The excitation spectra obtained upon analysis of the red Eu^{III} emission show a steady decrease in the spectral range attributable to the f–f excitation of Eu^{III} as one goes from pure Eu-mbzimpy **4** to Eu-doped Gd-mbzimpy (2%, 1%, 0.1%) to 'pure' Gd-mbzimpy **5**.

In addition to the lines associated with Eu^{III}, the emission spectrum of **5** displays a broad band identical to that observed for Lu-mbzimpy **7** and assigned to mbzimpy fluorescence (*Fig. 8*). The relative intensity of this band is, however, significantly reduced on going from the Lu to the Gd complex **5**, indicating the presence of an efficient deactivation process in the Gd sample. Nevertheless, the presence of Eu^{III} traces acting as killer sites is probably not the only reason for such an effect, and Gd^{III} levels probably play a role in the deactivation processes [42].

When the temperature is lowered (77 K and 4.2 K), the emission spectra measured upon ligand excitation for mbzimpy (**1**) and the Ln-mbzimpy complexes **5** (Ln = Gd) and **7** (Ln = Lu) (*Fig. 9*) display additional structured emission bands situated at lower energy than the $^1\pi\pi^*$ fluorescence bands observed at room temperature (zero phonon max. at

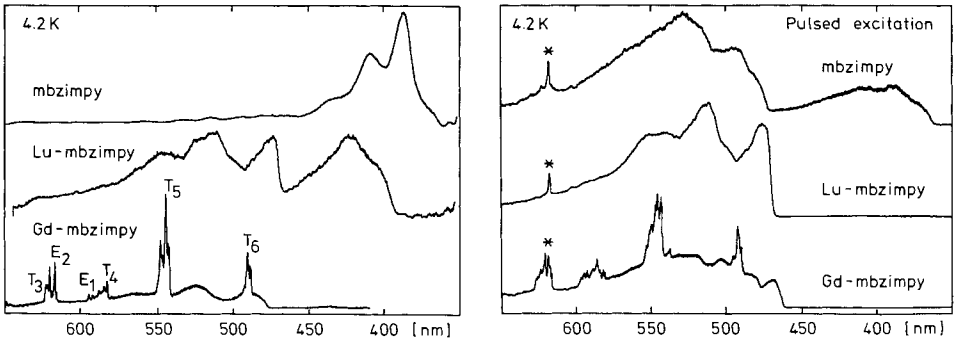

Fig. 9. *Emission spectra of mbzimpy* (**1**), *[Lu(mbzimpy)(NO$_3$)$_3$(CH$_3$OH)]* (**7**), *and [Gd(mbzimpy)(NO$_3$)$_3$(CH$_3$OH)]* (**5**) *at 4.2 K* ($E_J = {}^5D_0 \rightarrow {}^7F_J$ (Eu) transitions; $T_J = {}^5D_4 \rightarrow {}^7F_J$ (Tb) transitions). *Left*: excitation through continuous light source (Xe lamp) at 380 nm (free ligand) or 400 nm (complexes). *Right*: Pulsed excitation at 308 nm increasing I_{rel} of the long living signals (*: 2nd-order diffusion).

21300 cm^{-1}). Originating from long-living excited states (*Fig. 9b*, and *Table 4*), these bands are attributed to $^3\pi\pi^*$ phosphorescence. Similarly to τ_{obs}, the measured phosphorescence ratio increases, when temperature is lowered, but the $^1\pi\pi^*$ fluorescence bands observed in free mbzimpy (**1**) and **7** do not vanish at 4.2 K. This fact indicates a lower intersystem crossing rate for the ligand **1** than that reported (> 95%) for 2,2′-bipyridine cryptates [41].

Table 4. *Luminescence Lifetimes of the Ligand Triplet State* ($^3\pi\pi^*$)

Compound	λ_{exc} [nm]	λ_{an} [nm]	τ_{77K} [ms]	τ_{4K} [ms]
mbzimpy	308, 370	450	190 ± 10	323 ± 14
Lu-mbzimpy	308, 400	470, 520	87 ± 11	157 ± 4
Gd-mbzimpy	308, 400	470, 520	1.0 ± 0.2	7 ± 1

Similarly to bpy, the ligand exhibits a longer-living triplet state when uncomplexed. Furthermore, the triplet-state lifetime measured in Gd-mbzimpy **5** is considerably shorter than in Lu-mbzimpy **7**, confirming the role played by the paramagnetic Gd^{III} ion in the deactivation processes [42].

In addition to the surprising Eu emission previously observed at room temperature, the Gd-mbzimpy **5** spectra display Tb emission lines at low temperature, pointing to a thermal dependence of the energy-transfer processes. Since no similar effects are measured with the Gd-obzimpy **9**, these transfers are thought to arise from the peculiar packing found in the crystal structure of **4** which may favor energy-migration processes in the solid state (*vide infra*).

Luminescence of Ln^{III} Probes in Solid Samples. a) *Luminescence of Eu^{III} in mbzimpy and obzimpy Complexes. Fig. 10* (right) shows the excitation spectra observed upon analyzing the red emission of Eu^{III} in [Eu(mbzimpy)(NO$_3$)$_3$(CH$_3$OH)] (**4**) and [Eu(obzimpy)(NO$_3$)$_3$] (**8**) at 295 K. Both spectra are dominated by a strong broad band centered at *ca.* 395 nm and ascribed to ligand→Eu energy transfer [41]; the sharp lines located on

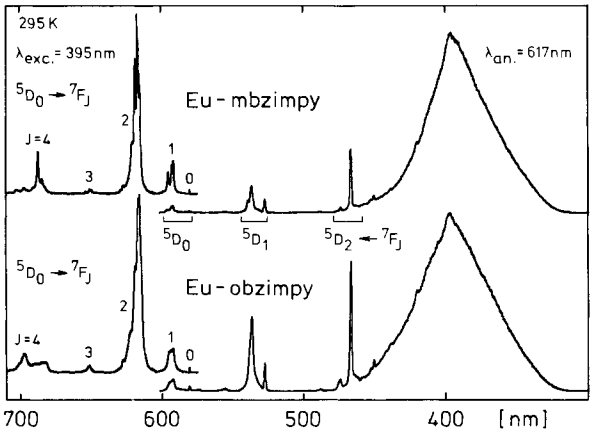

Fig. 10. *Luminescence spectra of [Eu(mbzimpy)(NO$_3$)$_3$(CH$_3$OH)]* (**4**) *and [Eu(obzimpy)(NO$_3$)$_3$]* (**8**) *microcrystalline samples at 295 K. Left*: emission spectra (ligand excitation at 395 nm); *right*: excitation spectra (analysis at 617 nm on the $^5D_0 \rightarrow {}^7F_2$ transition).

the low-energy side correspond to direct excitation of Eu^{III} on its ^5D_J levels. Similarly to the excitation spectra of free-mbzimpy and Gd- or Lu-mbzimpy complexes, the line shape of these spectra suffers from artefacts (*vide supra*).

Nonselective excitation at 395 nm (*via* ligand) gives emission spectra (*Fig. 10*, left) displaying the characteristic shape associated with $^5D_0 \rightarrow {}^7F_J$ transitions. Both spectra reflect low site symmetries: observable $^5D_0 \rightarrow {}^7F_0$ transition, maximum splitting for each ^7F_J levels ($2J + 1$), and intense hypersensitive $^5D_0 \rightarrow {}^7F_2$ transition. The relative and corrected intensities of the $^5D_0 \rightarrow {}^7F_J$ transitions for $J = 0$, 1, 2, 3, and 4 amount to 0.01, 1.0, 6.3, 0.3, and 2.4 for **4** and to 0.02, 1.0, 9.0, 0.3, and 2.1 for **8**. The broader lines observed in the spectrum of **8** indicate some fluxionality in the coordination geometry of Eu^{III}, in agreement with the larger residuals of the final *Fourier* analysis observed in the X-ray crystal structure of **8**.

Emission spectra identical to those of **4** were measured for all the Eu-doped Gd-, Tb-, and Lu-mbzimpy complexes, and even for the pure Gd- (**5**) or Tb-mbzimpy (**6**) complexes, demonstrating the isostructurality of all these compounds. The spectra show no evidence for any phase transition in the crystals upon varying the temperature from 295 K to 4.2 K.

Luminescence lifetimes of the $^5D_0$(Eu) level are reported on *Table 5* for pure and doped compounds at several temperatures. The values of τ_{obs} are temperature-indepen-

Table 5. *Luminescence Lifetimes of the $^5D_0$(Eu) and $^5D_4$(Tb) Levels in Ln-mbzimpy and Ln-obzimpy Complexes*

Compound	λ_{exc} [nm]	λ_{an} [nm]	τ_{295K} [ms]	τ_{77K} [ms]	τ_{4K} [ms]
Eu-mbzimpy[a])	308, 400	617	0.82 ± 0.04	0.84 ± 0.04	0.86 ± 0.05
Eu-obzimpy	308, 400	617	1.11 ± 0.04	1.12 ± 0.03	1.15 ± 0.05
Eu-obzimpy[b])	308, 400	617	1.70 ± 0.09	–	–
Tb-mbzimpy[a])	308, 400	544	0.101 ± 0.004	1.17 ± 0.05	1.22 ± 0.06

[a]) Pure compounds or 2% doped in Lu or Gd complexes.
[b]) Solution 10^{-3} M in CH_3CN.

dent and similar to those reported for tris-bpy cryptates in aqueous solution [41] [42]. The difference between **4** and **8** can be essentially related to the presence of CH_3OH around Eu^{III} in the former sample. Indeed, high-energy vibrations of OH oscillators deactivate efficiently the $^5D_0$(Eu) level through phonon-assisted vibrational coupling [1].

b) *Luminescence of Tb^{III} in mbzimpy Complexes.* Upon monitoring the green luminescence of Tb^{III} at 544 nm ($^5D_4 \rightarrow {}^7F_5$ transition), the excitation spectrum of $[Tb(mbzimpy)(NO_3)_3(CH_3OH)]$ (**6**) displays an intense broad band, similar to that observed for the Eu complex and corresponding to mbzimpy excitation followed by a ligand→Tb energy transfer. Direct excitation of Tb^{III} is also observed through a weak component centered around 490 nm ($^5D_4 \leftarrow {}^7F_6$ transition).

At 295 K, excitation *via* the ligand→Tb transfer band (395 nm) gives the emission spectrum reported in *Fig. 11, a* (upper spectrum). As already noticed for Gd-mbzimpy **5** (*vide supra*), emission lines originating from traces of Eu^{III} are observed along with those of Tb^{III} ($^5D_4 \rightarrow {}^7F_J$ transitions). Since the intensity of the Eu emission is comparable to that of the Tb emission in spite of its very low concentration, the presence of an extremely efficient mbzimpy→Eu energy-transfer process is confirmed. Since an intramolecular transfer process seems insufficient to produce such an intense luminescence with so few emitting species (< 0.01%), we suggest that a migration of the excited states among the mbzimpy units is responsible for this effect [41]. The stacking interaction found between the pyridine ring and the benzimidazole moieties of different ligands in the crystal structure of complex **4** strongly supports the possibility of such delocalized excited states.

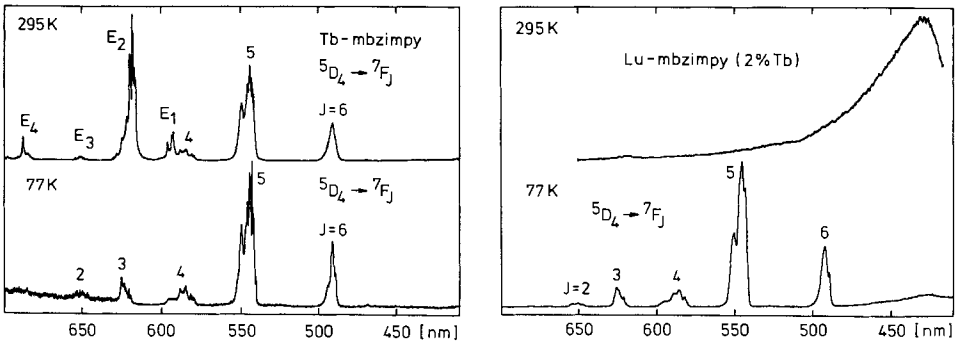

Fig. 11. *Emission spectra of [Tb(mbzimpy)$(NO_3)_3(CH_3OH)$] (left) and Tb^{3+}-doped (2%) [Lu(mbzimpy)$(NO_3)_3(CH_3OH)$] (right) upon ligand excitation at 395 nm ($E_J = {}^5D_0 \rightarrow {}^7F_J$ (Eu) transitions)*

The emission spectra recorded at 77 K (*Fig. 11*) point to another interesting characteristic: the strong thermal dependence of the Tb^{III} emission produced after ligand excitation. Such an effect has been observed previously [41] [42] and can be traced back to a thermally activated $^5D_4$(Tb) to $^3\pi\pi^*$(ligand) back transfer (minimal energy gap *ca.* 600 cm^{-1}), leading to the quenching of the $^5D_4$ luminescence as the temperature is raised. This statement is confirmed by luminescence lifetimes reported in *Table 5*.

c) *Energy-Transfer Processes.* The energy level scheme reported in *Fig. 12* summarizes the intramolecular processes taking place in $[Ln(mbzimpy)(NO_3)_3(CH_3OH)]$.

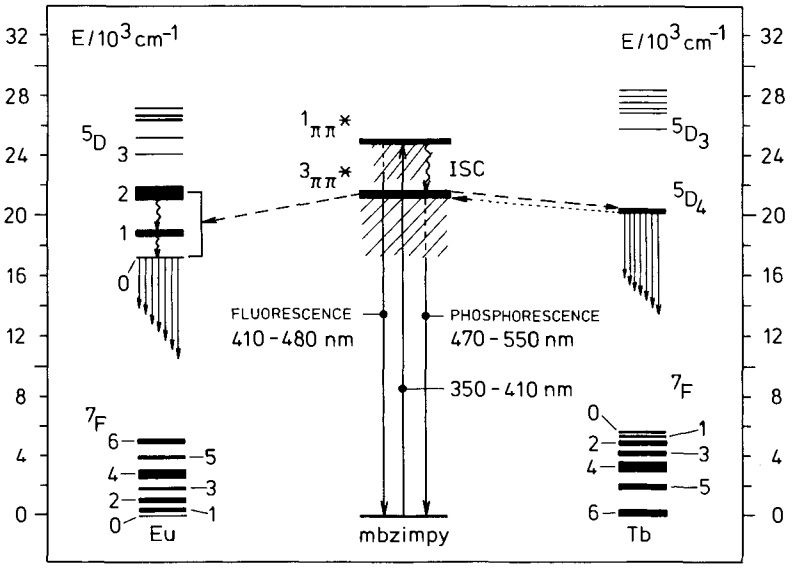

Fig. 12. *Energy-level diagram and energy-transfer scheme in [Ln(mbzimpy)(NO₃)₃(CH₃OH)] crystals*

A *ligand-to-Eu energy transfer* occurs from the $^3\pi\pi^*$ excited state of mbzimpy to the $^5D_2$, $^5D_1$, or $^5D_0$ levels of the Eu ion. Since the $^5D_2$ and $^5D_1$ excited levels are efficiently deactivated to $^5D_0$ through nonradiative processes (no emission originating from $^5D_2$ or $^5D_1$ is observed at 295 K), any back transfer similar to the one observed with Tb^{III} is precluded (energy gap *ca.* 4000 cm^{-1}). Moreover, the presence of an efficient migration of the ligand triplet state through several molecules could explain the surprisingly strong Eu^{III} luminescence observed even at very low Eu content (< 0.01%). This explanation is supported by the change in the relative intensity of the Eu^{III} emission as a function of temperature (*Fig. 13*). A decrease in temperature normally reduces the efficiency of

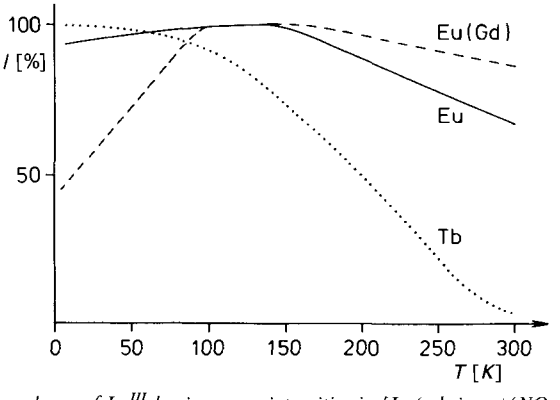

Fig. 13. Temperature dependance of Ln^{III} luminescence intensities in [Ln(mbzimpy)(NO₃)₃(CH₃OH)] cryptates (I_{rel} normalized to 100). *Full line*: Eu^{3+} in [Eu(mbzimpy)$(NO_3)_3$$(CH_3OH)$] (**4**); *dashed line*: Eu^{3+} in [Gd(mbzimpy)$(NO_3)_3$$(CH_3OH)$] (**5**); *dotted line*: Tb^{3+} in [Tb(mbzimpy)$(NO_3)_3$$(CH_3OH)$] (**6**).

nonradiative and other quenching processes, and leads to an exaltation of the luminescence, *cf.* Eu-mbzimpy sample (*Fig. 13*, full line). Surprisingly, this effect is not observed in the Gd-mbzimpy complex **5** (*Fig. 13*, dashed line). We explain this finding by the fact that the migration process of the ligand excited state is thermally activated: the triplet quenching increases with temperature (*cf.* τ_{obs} in *Table 5*). Cooling the sample down to 4.2 K reduces the migration rate, and the Eu emission becomes less intense.

Finally, it is interesting to note that energy-transfer processes in mbzimpy complexes lead to a strong Eu luminescence, contrary to what is observed in Ln-tris-bpy cryptates [42]. This can be attributed to the absence of any ligand-to-metal charge transfer (LMCT) band which could efficiently deactivate both the $^1\pi\pi^*$ and $^3\pi\pi^*$ excited levels.

Similarly, a *ligand-to-Tb energy transfer* takes place from the $^3\pi\pi^*$ excited state of mbzimpy to the $^5D_4$ level of the Tb ion. Again, migration of the ligand triplet state could explain the strong Tb emission observed in the Gd-mbzimpy complex at low temperature. Tb luminescence is, however, strongly reduced at room temperature, since a thermally activated Tb-to-ligand back-transfer mecanism (*vide supra*) is taking place: at room temperature, the small energy gap between $^3\pi\pi^*$ and $^5D_4$ (*ca.* 600 cm^{-1}), along with the relative lifetimes of these excited states, lead to an efficient quenching of the Tb luminescence *via* nonradiative deactivation of the ligand triplet states (*cf.* $\tau_{(^3\pi\pi^*)}$ *vs.* T in *Table 4*). At low temperature, nonradiative deactivation of the $^3\pi\pi^*$ level is reduced, and this back transfer is progressively inhibited, leading to a rise in Tb emission (*Fig. 13*).

In agreement with the proposed energy-migration scheme, a two-step *Tb → mbzimpy → Eu intermolecular process* is observed at room temperature in [Gd(mzimpy)-$(NO_3)_3(CH_3OH)$] (**5**) (99.99% Gd or doped with 2% Tb): the Eu emission produced by exciting the $Tb(^5D_4 \leftarrow {}^7F_6)$ transition at 488 nm increases as the Tb content increases. Any significant contribution of a direct *Tb → Eu* energy transfer can be precluded in view of the low doping rate of these samples (< 2% Tb; < 0.01% Eu).

Structure of the [Ln(obzimpy)(NO$_3$)$_3$] Complexes in Solution. To establish the structure of these complexes in solution, we have studied their absorption, emission, and ^{1}H-NMR spectra in MeCN.

The absorption spectra of free ligands mbzimpy (**1**) and obzimpy (**2**) in solution display a strong $\pi_1 \rightarrow \pi^*$ transition centered at 31150 cm^{-1}, blue-shifted with respect to the transition observed in the reflectance spectrum of **1**. As previously described in the solid state, coordination of Eu^{III} splits the $\pi_1 \rightarrow \pi^*$ transition into two components ($\pi_1^a \rightarrow \pi^*$ and $\pi_1^b \rightarrow \pi^*$, *Table 6*) suggesting a meridional coordination of obzimpy to the metal ion in solution [14] [34].

Table 6. *Electronic Absorptions of Free Ligands and Complexes in Solution*[a])

Compound	Solvent	$\pi_1^a \rightarrow \pi^*$	$\pi_1 \rightarrow \pi^*$	$\pi_1^b \rightarrow \pi^*$
mbzimpy	PC		31150 (32000)	
obzimpy	PC		31150 (30000)	
$[Eu(obzimpy)]^{3+}$	PC	32150 (24500)		29850 (21800)
$[Eu(obzimpy)]^{3+}$	CH_3CN	32570 (23200)		29070 (24300)
$[Cu(mbzimpy)]^{2+}$	PC [14]	31850 (23500)		27470 (16000)
$[Zn(mbzimpy)]^{2+}$	PC [14]	32570 (23500)		28330 (21500)

[a]) Energies in cm^{-1}, given for the maximum of the transition; PC = propylene carbonate. Molar absorption coefficients [M^{-1} cm^{-1}] are given in parentheses.

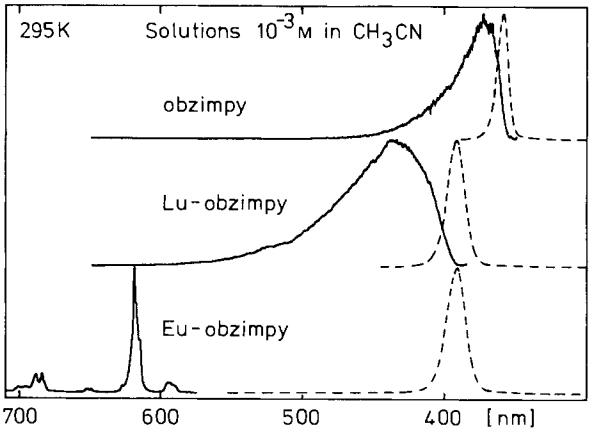

Fig. 14. *Luminescence spectra of obzimpy* (**2**), *[Lu(obzimpy)(NO$_3$)$_3$]* (**10**), *and [Eu(obzimpy)(NO$_3$)$_3$]* (**8**) (10^{-3} M solutions in CH_3CN at 295 K). *Full lines*: emission spectra (λ_{exc} = 385 nm (free ligand) and 425 nm (complexes)); *dashed lines*: excitation spectra (λ_{an} = 385 nm (free ligand), 425 nm (Lu-obzimpy), and 617 nm (Eu-obzimpy)).

Upon UV excitation, solutions of **2** and [Ln(obzimpy)(NO$_3$)$_3$] complexes **8** (Ln = Eu) and **10** (Ln = Lu) (10^{-3} M) give the emission spectra reported in *Fig. 14* (full line). The ligand emission broad bands observed in the spectra of **2** and [Lu(obzimpy(NO$_3$)$_3$] (**10**) display shapes and maxima similar to those observed in the spectra of **1** and Lu-mbzimpy **7** crystalline samples (*cf. Fig. 8*). This precludes any large change in the electronic levels of the ligand upon dissolution. Moreover, inspection of the Eu emission spectra for [Eu(obzimpy)(NO$_3$)$_3$] (**8**) both in solution and in the solid state (*cf. Fig. 10*) reveals a similar chemical environment for the metal ion.

Broad-band excitation spectra measured by analyzing the ligand emission (*Fig. 14*, dashed lines) display one single band assigned to excitation through the obzimpy $^1\pi\pi^*$ level. This band is narrower than in the spectra of the coresponding crystalline samples, with a maximum situated at lower wavelength.

Analyzing the Eu^{III} red luminescence (617 nm) in the solution of **8** gives the same excitation spectrum as previously observed for complex **10**, showing an efficient obzimpy→Eu energy transfer which suggests that the Eu^{III} sites retain their coordination to obzimpy and confirms the stability of these complexes in solution. In spite of the observation of two species in solution by ^{1}H-NMR (*vide infra*), selective excitation of the profile of the broad $^5D_0 \leftarrow {}^7F_0$ band gives no evidence for different Eu^{III} sites.

The ^{1}H-NMR spectra of the tridentate ligands mbzimpy (**1**) and obzimpy (**2**) show pseudo-first-order signals for the pyridine protons H_3, H_5, and a complicated *ABCD* spin system for the benzimidazole protons H_1–H_4 with H_1 giving a *multiplet* around 7.8 ppm and the other three protons a *multiplet* between 7.3 and 7.5 ppm [15].

Upon complexation to Lu^{III} in complex **10**, the pyridine protons still display pseudo-first-order spectra, but at lower field for H_6 (0.49 ppm) which is typical for N-coordination of the pyridine ring [15] [44]. As previously reported for Zn^{II} [14] and Cu^{I} [15], the ^{1}H-NMR signals of the benzimidazole protons H_1–H_4 are only slightly modified by the complexation to give a pseudo-first-order spectrum at slightly lower field in complex **10**. However, the multiplicities of these signals do not correspond to the expected pseudo-

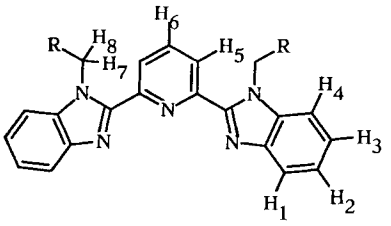

1 (mbzimpy) R = H

2 (obzimpy) R = $CH_3(CH_2)_6$

doublet (H_1,H_4)and pseudo-*triplet* patterns (H_2,H_3) which strongly support a mixture of quite similar complexes in solution. To investigate further the different complexes formed in MeCN, we have used the Eu^{III} paramagnetic probe in complex **8** [45]. The ^{1}H-NMR spectrum of **8** in CD_3CN clearly shows an approximately 1:1 mixture (47%:53%) of two different complexes which do not exchange rapidly, and where obzimpy is symmetrically coordinated to Eu^{III} on the NMR time scale (*Table 7*). The attribution of the ^{1}H-NMR signals was performed by a two-dimensional homonuclear COSY correlation spectrum which also unambiguously confirms the existence of only two well-defined different complexes with very similar ^{1}H-NMR characteristics. Solvation processes, conformation equilibria, or partial decomplexation of NO_3 groups (bidentate↔monodentate) in MeCN could be responsible for the formation of two different species in solution.

Table 7. *^{1}H-NMR Chemical Shifts* (with respect to TMS) *for Ligands* **1**–**2** *in $CDCl_3$ and for Complexes* **8**, **10** *in CD_3CN*

Compound	Solvent	H_1	H_2	H_3	H_4	H_5	H_6	H_7, H_8
1	$CDCl_3$	7.8		7.3–7.5 (*m*)		8.42	8.05	4.25
2	$CDCl_3$	7.8		7.3–7.5 (*m*)		8.32	8.05	4.52
8	CD_3CN	18.6	10.3	9.49	8.14	5.12	6.32	5.10
		16.8	9.37	8.88	7.77	6.36	7.09	5.70
10	CD_3CN	8.15	7.5–7.6 (*m*)		7.9	8.35	8.54	4.68

Conclusions. – Both X-ray crystal structures of complexes [Eu(mbzimpy)-$(NO_3)_3(CH_3OH)$] (**4**) and [Eu(obzimpy)$(NO_3)_3$] (**8**) display the desired meridional coordination of the tridentate rigid aromatic mbzimpy (**1**) and obzimpy (**2**) ligands to the metal ion. Compared to the terpyridine analogue, the good fit observed between the coordination cavity and the size of mid-range Ln^{III} ions is confirmed by the persistence of the coordination in solution, as exemplified by ^{1}H-NMR and luminescence measurements.

The peculiar luminescent properties observed in the investigated complexes involve two main type of processes as energy transfer mechanisms: specific *intramolecular transfers* are responsible for conversion of the UV-light absorbed by both ligands **1** and **2** into visible light emitted by Eu^{III} or Tb^{III}. As observed through the significant temperature effect, the efficiency of such transfers is related to the spectral overlap of the donor and acceptor energy levels together with the relative lifetimes of these excited levels. The second type of process is a very efficient *intermolecular transfer*, as observed in

Gd-mbzimpy crystals where Eu^{III} and Tb^{III} impurities at level lower than 0.01% are observed. A stacking effect seems to favor delocalization of the ligand excited states, leading to the observed energy-migration processes through the crystal in $[Ln(mbzimpy)(NO_3)_3(CH_3OH)]$ complexes. This effect can be controlled by a small modification of the ligand as in $[Ln(obzimpy)(NO_3)_3]$ which does not significantly affect the coordination sphere around the metal ion, but drastically changes the intermolecular interaction in the crystal.

The photophysical results reported here are in agreement with the interpretation published for Ln-tris-bpy cryptate studies [41] [42], but the consideration of intramolecular and intermolecular interactions in Ln^{III} complexes offers new possibilities in the field of ligand design for efficient light conversion.

We thank Ms. *Véronique Foiret* and Mr. *Bernard Bocquet* for their technical assistance. *E.M.* and *J.-C.B.* thank the *Fondation Herbette* (Lausanne) for the gift of spectroscopic equipment. This work is supported through grants from the *Swiss National Science Foundation*.

REFERENCES

[1] G.R. Choppin, J.-C.G. Bünzli, 'Lanthanide Probes in Life, Medical and Environmental Sciences', Elsevier Publishing Co., Amsterdam, 1989, Chapt. 7.

[2] M. Pietraskiewicz, S. Pappalardo, P. Finocchiano, A. Mamo, J. Karpiuk, *J. Chem. Soc., Chem. Commun.* **1990,** 1907; V. Balzani, J.-M. Lehn, J. Van Loosdrecht, A. Mecati, N. Sabbatini, R. Ziessel, *Angew. Chem. Int. Ed.* **1991,** *30,* 190.

[3] B. Alpha, J.-M. Lehn, G. Mathis, *Angew. Chem. Int. Ed.* **1987,** *26,* 266; B. Alpha, V. Balzani, J.-M. Lehn, S. Perathoner, N. Sabbatini, *ibid.* **1987,** *26,* 1266; J.-M. Lehn, M. Pietraszkiewicz, J. Karpiuk, *Helv. Chim. Acta* **1990,** *73,* 106; N. Sabbatini, A. Mecati, M. Guardigli, V. Balzani, J.-M. Lehn, R. Ziessel, R. Ungaro, *J. Lumin.* **1991,** *48–49,* 463.

[4] V. Balzani, E. Berghmans, J.-M. Lehn, N. Sabbatini, A. Mecati, R. Therorde, R. Ziessel, *Helv. Chim. Acta* **1990,** *73,* 2083; L. Prodi, M. Maestri, R. Ziessel, V. Balzani, *Inorg. Chem.* **1991,** *30,* 3798.

[5] J.-C.G. Bünzli, in 'Handbook on the Physics and Chemistry of Rare Earths, Eds. K.A. Gschneidner, Jr. and L. Eyring, Elsevier, Amsterdam, 1987, Vol. 9, Chapt. 60.

[6] D.W. Fink, W.E. Ohnesorge, *J. Phys. Chem.* **1970,** *74,* 72; S.P. Sinha, *Z. Naturforsch., A* **1965,** *20,* 835.

[7] E.C. Constable, *Adv. Inorg. Chem. Radiochem.* **1986,** *30,* 69.

[8] L.J. Basille, D.L. Gronert, J.R. Ferraro, *Spectrochim. Acta, Part A* **1968,** 707; L.R. Melby, N.J. Rose, E. Abramson, J.C. Caris, *J. Am. Chem. Soc.* **1964,** *86,* 5117, S.P. Sinha, *Z. Naturforsch., A* **1965,** *20,* 1661: S.P. Sinha, *ibid.* **1965,** *20,* 552.

[9] S.P. Sinha, *Z. Naturforsch., A* **1965,** *20,* 164.

[10] R.C. Holz, L.C. Thomson, *Inorg. Chem.* **1988,** *27,* 4640.

[11] D.A. Durham, G.H. Frost, F.A. Hart, *J. Inorg. Nucl. Chem.* **1969,** *31,* 833; G.H. Frost, F.A. Hart, M.B. Hursthouse, *J. Chem. Soc., Chem. Commun.* **1969,** 1421.

[12] R.D. Chapman, R.T. Loda, J.P. Riehl, R.W. Schwartz, *Inorg. Chem.* **1984,** *23,* 1652.

[13] J.-P. Sauvage, M.D. Ward, *Inorg. Chem.* **1991,** *30,* 3869.

[14] C. Piguet, B. Bocquet, E. Müller, A.F. Williams, *Helv. Chim. Acta* **1989,** *72,* 323.

[15] C. Piguet, G. Bernardinelli, A.F. Williams, *Inorg. Chem.* **1989,** *28,* 2920; S. Rüttimann, C. Piguet, G. Bernardinelli, B. Bocquet, A.F. Williams, *J. Am. Chem. Soc.,* **1992,** *114,* 4230.

[16] C. Piguet, Ph.D. Thesis No. 2385, Faculty of Sciences, University of Geneva, 1989.

[17] A.F. Williams, C. Piguet, G. Bernardinelli, *Angew. Chem. Int. Ed.* **1991,** *30,* 1490; C. Piguet, G. Bernardinelli, B. Bocquet, A. Quattropani, A.F. Williams, *J. Am. Chem. Soc.*, in press.

[18] P. Guerriero, P.A. Vigato, J.-C.G. Bünzli, E. Moret, *J. Chem. Soc., Dalton Trans.* **1990,** 647.

[19] J.-C.G. Bünzli, J.-R. Yersin, *Inorg. Chem.* **1979,** *18,* 605.

[20] E. Blanc, D. Schwarzenbach, H.D. Flack, *J. Appl. Crystallogr.* **1991,** *24,* 1035.

[21] P. Main, S.J. Fiske, S.E. Hull, L. Lessinger, D. Germain, J.P. Declercq, M.M. Woolfson, 'MULTAN 87', Universities of York, England, and Louvaine-La-Neuve, Belgium, 1987.

[22] S. R. Hall, J. M. Stewart, Eds., 'XTAL 3.0 User's Manual', Universities of Western Australia and Maryland, 1989.
[23] C. K. Johnson, 'ORTEP II', Report ORNL-5138, Oak Ridge National Laboratory, Oak Ridge, Tennessee, 1976.
[24] 'International Tables for X-Ray Crystallography, Kynoch Press, Birmingham, 1974, Vol. IV.
[25] G. Bernardinelli, H. D. Flack, *Acta Crystallogr., Sect. A* **1985,** *41,* 500.
[26] J. C.-G. Bünzli, G.-O. Pradervand, *J. Chem. Phys.* **1986,** *85,* 2489; J.-C. G. Bünzli, G. A. Leonard, D. Plancherel, G. Chapuis, *Helv. Chim. Acta* **1986,** *69,* 288; J.-C. G. Bünzli, D. Plancherel, G.-O. Pradervand, *J. Phys. Chem.* **1989,** *93,* 980; J.-C. G. Bünzli, E. Moret, U. Casellato, P. Guerriero, P. A. Vigato, *Inorg. Chim. Acta* **1988,** *150,* 133; E. Moret, F. Nicolò, D. Plancherel, P. Froidevaux, J.-C. G. Bünzli, G. Chapuis, *Helv. Chim. Acta* **1991,** *74,* 65.
[27] K. Nakamoto, 'Infrared and Raman Spectra of Inorganic and Coordination Compounds', 3rd edn., John Wiley, New York–Chichester–Brisbane–Toronto, 1972, p. 244.
[28] F. Scheinmamm, 'An Introduction to Spectroscopic Methods for the Identification of Organic Compounds', Pergamon Press, Oxford–New York–Toronto–Sydney–Braunschweig, 1970, Vol. 1, p. 173.
[29] C. C. Addison, N. Logan, S. C. Wallwork, C. D. Garner, *Quart. Rev.* **1971,** *25,* 289.
[30] A. B. P. Lever, E. Mantovani, B. S. Ramaswamy, *Can. J. Chem.* **1971,** *49,* 1957.
[31] S. B. Sanni, H. J. Behm, P. T. Beurskens, G. A. van Albada, J. Reedijk, A. T. H. Lenstra, A. W. Addison, M. Palaniandavar, *J. Chem. Soc., Dalton Trans.* **1988,** 1429; G. Bernardinelli, A. F. Williams, G. Hopfgartner, *Acta Crystallogr., Sect. C* **1990,** *46,* 1642.
[32] K. Nakamoto, *J. Phys. Chem.* **1960,** *64,* 1420.
[33] E. C. Constable, J. Lewis, M. C. Liptrot, P. R. Raithby, *Inorg. Chim. Acta* **1990,** *178,* 47.
[34] S. Rüttimann, G. Bernardinelli, C. M. Moreau, A. F. Williams, A. W. Addison, *Polyhedron* **1992,** *11,* 635.
[35] R. D. Shannon, *Acta Crystallogr., Sect. A* **1976,** *32,* 751.
[36] E. Moret, J.-C. G. Bünzli, K. J. Schenk, *Inorg. Chim. Acta* **1990,** *178,* 83.
[37] M. Sakamoto, M. Matsumoto, H. Okawa, *Bull. Chem. Soc. Jpn.* **1991,** *64,* 691.
[38] F. A. Cotton, G. Wilkinson, 'Advanced Inorganic Chemistry', 5th edn., John Wiley, New York–Chichester–Brisbane–Toronto–Singapore, 1988, p. 90; M. D. Joesten, *J. Chem. Educ.* **1982,** *59,* 362.
[39] M. H. Chisholm, J. C. Huffman, I. P. Rothwell, P. G. Bradley, N. Kress, W. H. Woodruff, *J. Am. Chem. Soc.* **1981,** *103,* 4945.
[40] E. C. Constable, S. M. Elder, J. A. Healy, D. A. Tocher, *J. Chem. Soc., Dalton Trans.* **1990,** 1010.
[41] G. Blasse, G. J. Dirksen, N. Sabbatini, S. Perathoner, J.-M. Lehn, B. Alpha, *J. Phys. Chem.* **1988,** *92,* 2419: G. Blasse, G. J. Dirksen, D. Van Der Voort, N. Sabbatini, S. Perathoner, J.-M. Lehn, B. Alpha, *Chem. Phys. Lett.* **1988,** *146,* 347.
[42] B. Alpha, R. Ballardini, V. Balzani, J.-M. Lehn, S. Perathoner, N. Sabbatini, *Photochem. Photobiol.* **1990,** *52,* 299.
[43] I. Bkouche-Waksman, J. Guilhem, C. Pascard, B. Alpha, R. Deschenaux, J.-M. Lehn, *Helv. Chim. Acta* **1991,** *74,* 1163.
[44] D. K. Lavallee, M. D. Baughman, M. P. Phillips, *J. Am. Chem. Soc.* **1977,** *99,* 718.
[45] I. Bertini, C. Luchinat, 'NMR of Paramagnetic Molecules in Biological Systems', Benjamin/Cummings Publishing Co., Inc., 1986, Chapt. 10.